

## High- $\beta$ Plasmas in the PBX Tokamak

K. Bol, D. Buchenauer,<sup>(a)</sup> M. Chance, P. Couture,<sup>(b)</sup> H. Fishman, R. Fonck, G. Gammel, B. Grek, K. Ida,<sup>(c)</sup> K. Itami,<sup>(c)</sup> K. Jaehnig, G. Jahns,<sup>(d)</sup> D. Johnson, R. Kaita, S. Kaye, H. Kugel, B. LeBlanc, J. Manickam, K. McGuire, N. Ohyabu,<sup>(d)</sup> M. Okabayashi, E. Powell, M. Reusch, G. Schmidt, S. Sesnic, H. Takahashi, and F. Tenney<sup>(e)</sup>

Princeton Plasma Physics Laboratory, Princeton University, Princeton, New Jersey 08544

(Received 3 March 1986)

Bean-shaped configurations have been successfully formed in the PBX tokamak and  $\beta$  values of over 5% have been obtained. These discharges still lie in the first stability regime for ballooning modes, and magnetohydrodynamics stability analysis implicates the external kink as responsible for the present  $\beta$  limit.

PACS numbers: 52.55.Fa

To be interesting to a tokamak-fusion-reactor designer, the ratio of plasma to toroidal magnetic field pressure,  $\beta$ , should be at least 10%,<sup>1</sup> a value well in excess of the approximately 3% limit observed in (nearly) circular-cross-section tokamaks,<sup>2</sup> or the 4.5% reached in elongated Doublet III plasmas.<sup>3</sup> The experimental  $\beta$  limit agrees remarkably well with a scaling developed by Troyon *et al.*,<sup>4</sup> for which the destabilization of an  $n=1$  ideal external kink mode is the limiting factor. According to Ref. 4,  $\beta \leq c\beta_c$ , where  $\beta_c \equiv \mu_0 I_p / a_{\text{mid}} B_t$ ,  $I_p$  is the plasma current,  $a_{\text{mid}}$  the plasma half-width on the midplane, and  $B_t$  the toroidal field at the geometric center. The coefficient is given as  $c=2.2$ . A similar scaling but with a 50% larger coefficient  $c$  has been obtained by Sykes, Turner, and Patel<sup>5</sup> in a stability investigation of ballooning modes.

While the long-wavelength external kink mode can, in principle, be stabilized by surrounding the plasma with a sufficiently close-fitting conducting shell, the internal kink or ballooning modes cannot. However, at sufficiently high  $\beta$  (and not too small aspect ratio, e.g.,  $R/a \geq 4$ ) a second region of ballooning stability exists<sup>6</sup>—the problem is to get to it. Indenting the plasma cross section on the small-major-radius side has long been predicted to enhance magnetohydrodynamics (MHD) stability against localized pressure-driven, flute-like modes,<sup>7-10</sup> and indeed, more recent numerical work has shown that such indentation, or “bean” shaping, enhances the stability of the plasma to not only the short-wavelength internal kink. In fact, with sufficient indentation and appropriately constrained pressure and current profiles, the second stability region for both types of modes is directly accessible.<sup>11,12</sup> For a broader range of moderate-aspect-ratio equilibria the first stability limit is not eliminated, but raised above 10%—still a very attractive reactor regime.

To explore the merits of bean shaping for reaching high  $\beta$ , in particular the second stability region, the divertor tokamak PDX<sup>13</sup> was modified to PBX (Princeton beta experiment). However, a close-fitting,

kink-suppressing conducting shell was omitted (cf. Fig. 1) in the interest of simplicity and flexibility, in the belief that kinks could be circumvented by the same operational tricks that have allowed tokamak operation at values of the safety factor  $q \approx 2$ . (A further machine modification is currently under way to install such a shell.) Details of the modification and of the formation of bean-shaped plasmas are given elsewhere<sup>14</sup>; here we focus on the maximization of  $\beta$ , the

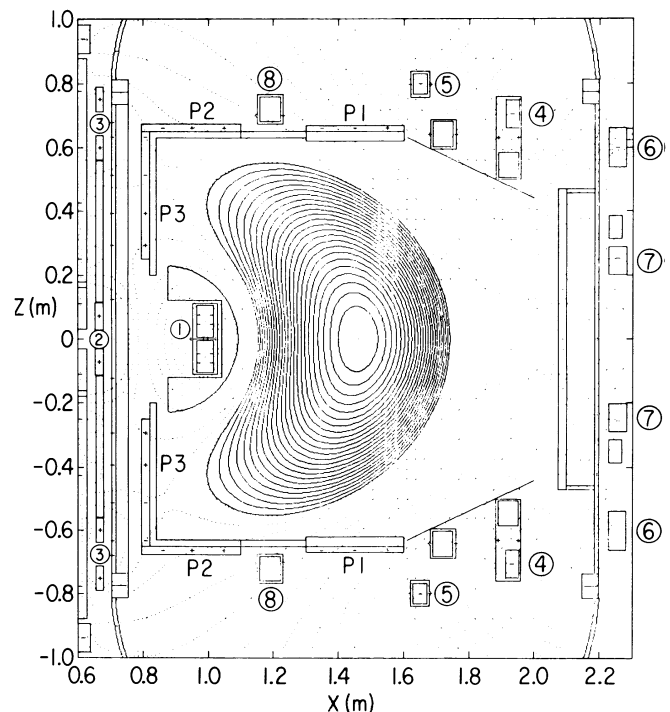


FIG. 1. Layout of PBX with magnetic field configuration for  $\beta=5\%$ . P1–P3 are the aluminum passive stabilizers; coils 1–4 do the shaping; coils 5–7 provide radial equilibrium. Graphite armor is shown on coil 1 and the thickness of the graphite bars on P1–P3.

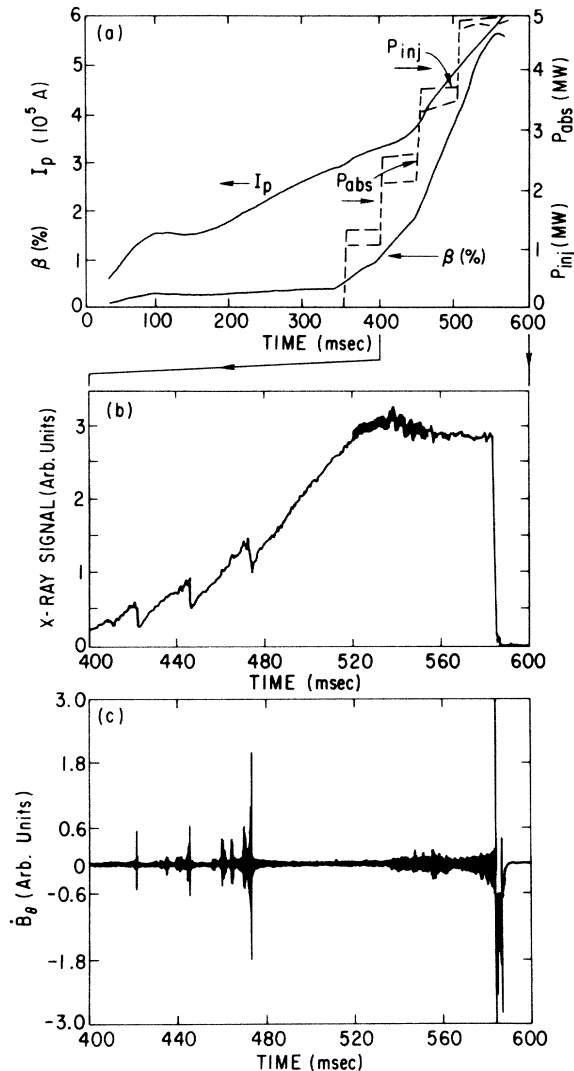


FIG. 2. Time behavior of plasma parameters for high  $\beta$ : (a) Plasma current  $I_p$ , injected power  $P_{inj}$ , absorbed power  $P_{abs}$ , and plasma  $\beta$ ; (b) x-ray signal on the horizontal plane; and (c) Mirnov signal  $\dot{B}_\theta$ .

core of the PBX experiment.

PBX plasmas are heated with four neutral beams each having a nominal rating for deuterium of 2 MW at 50 kV. All four beams are co-injected, two at a tangency radius of 35 cm and two at 130 cm. High- $\beta$  experiments are performed at low magnetic field strength ( $B_t = 0.8$ – $1.1$  T) in order to maximize  $\beta$  for given heating capacity, and with a fast plasma current rampup (2 MA/sec) to broaden the current profile via the skin effect. Discharges with peaked profiles need steeper shaping-field gradients to achieve the same indentation, which destabilizes the vertical plasma position, and they have weaker shaping of the internal flux surfaces. The indentation—defined as  $d/(d + 2a_{mid})$ , where  $d$  is the depth of the indentation relative to the

beam-tip position projected on the midplane—is typically about 20%.

Figure 2 shows a high- $\beta$  discharge obtained as described above.  $\beta$  as shown in Fig. 2(a) was calculated from formulas given by Shafranov,<sup>15</sup> with use as inputs the observed poloidal flux values, the diamagnetic flux, and plasma current. For this discharge, the value of  $\beta$  increases from 0.5% in the Ohmic phase to 5% with neutral-beam heating. Here  $\beta$  is defined as  $2\mu_0\langle p\rangle/\langle B_t^2\rangle$ , where  $p$  denotes the total pressure of beam and plasma, and the brackets denote a volume average. If instead  $\beta$  is defined by use of the value of  $B_t$  at the magnetic axis, the values are 10% higher. However, computing  $\beta$  in accordance with our definition over the D-shaped volume that includes the plasma-free indentation would lower  $\beta$  by about 14%.

This particular discharge disrupted at 580 msec, at which time the plasma current was 590 kA and the indentation was 0.20. The plasma parameters shown in Fig. 2, averaged over a 15-msec interval centered on 560 msec, are  $\beta = 5.3\%$ ,  $B_t = 0.9$  T,  $I_p = 570$  kA,  $dI_p/dt \approx 2$  MA/sec,  $q_\psi = 3$ , neutral-beam heating power = 4.7 MW, and stored energy = 160 kJ. A simple measure of current density is the “equivalent cylindrical  $q$ ,”  $q^*$ , where  $q^* \equiv \langle a \rangle B_t / R_{mag} B_p(a)$ ; here  $\langle a \rangle$  is the volume-average minor radius and  $B_p(a) \equiv (\mu_0/2\pi) I_p / \langle a \rangle$ . Typically in PBX,  $q^* \rightarrow 1$  while  $q_\psi \rightarrow 3$ . A value of  $q^* \approx 1.0$  is, to our best knowledge, the lowest which has been achieved in large tokamak experiments without further deterioration of energy-confinement properties below  $L$  mode, and is the basic reason for the success of the bean configuration in reaching high  $\beta$ .

The MHD behavior during the beam-injection phase is shown by soft-x-ray and Mirnov-probe signals [Figs. 2(b) and 2(c)]. After the last sawtooth occurs at 470 msec, the MHD activity detected by the Mirnov coils becomes very small and only shows a mild resurgence as  $\beta$  increases above 3%. Even then there is no hint of either sawteeth (sharp drop in soft-x-ray signal) or fishbones<sup>2</sup> (“spikes” in Mirnov signal,  $\dot{B}_\theta$ , in between sawteeth fluctuation spikes).

A kinetic documentation with a multipoint Thomson scattering system was carried out at  $\beta \approx 4.5\%$ , where plasma conditions are much more readily reproduced than at the highest betas. The operating conditions for these discharges were basically the same as for the shot of Fig. 2, but with a somewhat smaller plasma current (560 kA) and some trimming of the gas fueling rate. The temperature and density were reproducible to within 10%. Figure 3 shows time slices of  $T_e$  and  $n_e$  midplane profiles. The  $T_e$  profile, initially with  $T_e(0) = 1$  keV, recovers to a peaked profile within 20 msec after the last sawtooth crash and evolves to a final temperature profile with  $T_e(0) = 2.0$  keV, while the broadness is more or less maintained. The mag-

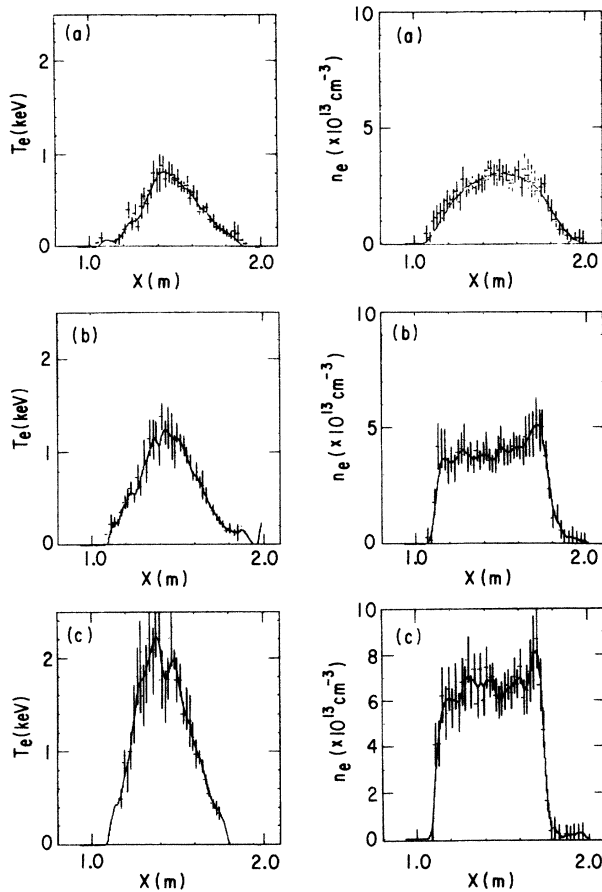


FIG. 3. Electron temperature and plasma density profiles (a) just after the initiation of neutral-beam injection (400 msec); (b) just after the last sawtooth (490 msec); and (c) just before the disruption (580 msec).

netic axis, as defined by the electron temperature peak, is made to shift inward from 1.46 to 1.43 m in order to increase the indentation from 0.14 at  $t=400$  msec to 0.18 at 580 msec. The density profile, initially rather peaked, becomes extremely flat with an outward asymmetry developing—behavior similar to that in the high-density mode in PDX.<sup>13</sup> The average density reaches  $(5-6) \times 10^{13} \text{ cm}^{-3}$ . The central ion temperature, measured from the Doppler broadening of charge-exchange-recombination light of fully stripped impurity ions, shows  $T_i(0)$  increasing to 4–5 keV and then saturating; this is probably due to the buildup of plasma density.

With use of the measured  $T_e(r,t)$  and  $n_e(r,t)$  profiles, a detailed analysis was carried out on this series of discharges. We find that at these densities the large difference between the measured  $T_e(0)$  and  $T_i(0)$  values cannot be supported by classical electron-ion coupling alone: Even with zero ion heat conduction at the center the computed  $T_i(0)$  is approximately 1 keV

less than the measured value. A possible candidate for the additional ion energy source needed to obtain a consistent energy balance is viscous damping by the ions of the high plasma rotation induced by the two tangential beams. Work is continuing on this topic. The equilibrium stored energy obtained from the kinetic calculation is 90% of that determined from the magnetics, with the difference exactly, but fortuitously, accounted for by the discrepancy in the computed and measured  $T_i$  values. The uncertainties in the transport calculations are also in the 10% range. The beam contribution to the total  $\beta$  is calculated to be 20%, while the electrons and ions each account for about 40%.

High- $\beta$  discharges frequently terminate in a so-called “high- $\beta$  disruption” at values typical for ideal kink modes.<sup>4</sup> To determine the MHD-stability limit more accurately for actual PBX discharge parameters, detailed numerical studies have been carried out. Self-consistent equilibria are constructed that satisfy the Grad-Shafranov equation with the experimental constraints: poloidal fluxes, diamagnetic flux, and external fields generated by both measured coil currents and calculated eddy currents. The profile of total plasma pressure is scaled from the electron pressure. The current profile is adjusted to match the total plasma current and the approximate location of the  $q=1$  surface, but with this parametrization the choice is tightly constrained by the data; i.e.,  $q(0)$  cannot be varied more than 10% without violating the experimental error limits on the input data.

The MHD stability of the high- $\beta$  equilibrium of Fig. 1 was investigated with the code<sup>16</sup> PEST and found to be unstable to the  $n=1$  external kink mode (conducting wall at infinity), but stable both to the  $n=1$  internal kink (conducting wall bounding the plasma) and to ballooning modes. Since  $1-q(0)$  is a sensitive parameter for these instabilities,  $q(0)$  was varied in the stability calculation by scaling of the toroidal field. As Fig. 4 illustrates, a variation of  $q(0)$  within the range of 0.8–0.9 has only a slight effect, whereas the presence of a conducting wall 1 plasma radius away would raise the critical  $\beta$  to the observed value. A closer wall could raise the kink limit above the ballooning limit.

The MHD oscillation observed at the time of disruption is characterized by  $n=1$  and  $m \geq 3$ , with a growth time of 100–150  $\mu\text{sec}$ . A detailed study of this mode, which will be published elsewhere, shows quite reasonable agreement between signals measured by an array of magnetic pickup coils and those calculated from PEST.

In conclusion, bean-shaped configurations have been investigated for their suitability in reaching high  $\beta$ . The ability of such shaped discharges to accommodate high mean current densities ( $q^* \approx 1$ ) has made  $\beta$ 's of 5% and over accessible within the usual first sta-

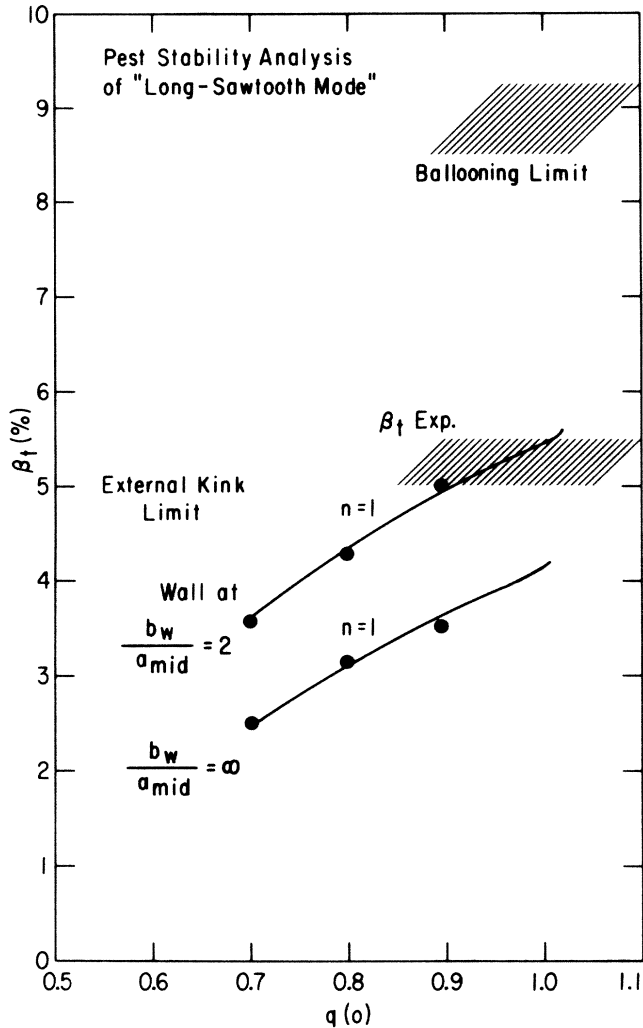


FIG. 4. Critical  $\beta$  vs  $q(0)$  from ideal MHD analysis.  $a_{\text{mid}}$  is the plasma width on the midplane and  $b_w$  is the wall location measured from the geometrical center on the midplane. The first stability limit for a ballooning mode of 8.5% is indicated by the shaded area. The maximum  $\beta$  achieved in PBX is (5.0–5.5)%.

bility limit. The mode which limits  $\beta$  has a long toroidal wavelength ( $n=1$ ) and fits the theoretical model for a free-boundary kink with a conducting wall located approximately 1 plasma radius away from the plasma boundary. This interpretation indicates that a more tightly fitting shell would raise the kink beta limit above the ballooning limit and allow a test of the bean shape as a means for achieving access to the second stable region for ballooning modes.

The authors would like to thank both the PBX technical operation crew headed by J. Semler and the neutral-beam group for their contributions to this

work, and P. Rutherford and H. P. Furth for their support and encouragement. This work was supported by the U. S. Department of Energy under Contract No. DE-AC02-76-CH03073.

(a)Permanent address: Sandia National Laboratory, Livermore, CA 87185.

(b)Permanent address: Institut de Recherche d'Hydro-Quebec, Canada.

(c)Permanent address: University of Tokyo, Tokyo, Japan.

(d)Permanent address: GA Technologies Inc., San Diego, CA.

(e)Deceased.

<sup>1</sup>J. Sheffield, Nucl. Fusion **25**, 1733 (1985).

<sup>2</sup>K. McGuire *et al.*, in *Plasma Physics and Controlled Nuclear Fusion Research, 1984* (IAEA, Vienna, 1985), Vol. 1, p. 117; M. Murakami *et al.*, *ibid.*, Vol. 1, p. 87; M. Keilhacker *et al.*, *ibid.*, Vol. 1, p. 71.

<sup>3</sup>R. D. Stambaugh *et al.*, in *Plasma Physics and Controlled Nuclear Fusion Research, 1984* (IAEA, Vienna, 1985), Vol. 1, p. 217.

<sup>4</sup>F. Troyon, R. Gruber, H. Sauremann, S. Semenzato, and S. Succi, Plasma Phys. Controlled Nucl. Fusion **26**, 209 (1984).

<sup>5</sup>A. Sykes, M. F. Turner, and S. Patel, in *Controlled Fusion and Plasma Physics* (European Physical Society, Aachen, 1983).

<sup>6</sup>J. M. Greene and M. S. Chance, Nucl. Fusion **21**, 4 (1981); B. Coppi, A. Ferreira, and J. J. Ramos, Phys. Rev. Lett. **44**, 990 (1980); C. Mercier, in *Plasma Physics and Controlled Nuclear Fusion Research, 1978* (IAEA, Vienna, 1979) Vol. 1, p. 701.

<sup>7</sup>H. P. Furth, J. Killeen, M. Rosenbluth, and B. Coppi, in *Plasma Physics and Controlled Nuclear Fusion Research, 1965* (IAEA, Vienna, 1966), Vol. 1, p. 103.

<sup>8</sup>V. Shafranov and E. Yurchenko, Nucl. Fusion **8**, 329 (1968); L. Solov'ev, Zh. Eksp. Teor. Fiz. **53**, 626 (1967) [Sov. Phys. JEPT **26**, 400 (1968)].

<sup>9</sup>C. Mercier, in Commission of European Communities Report No. EURATOM-CEA 5127e, 1974 (unpublished).

<sup>10</sup>K. Weimer, E. Rieman, and J. Johnson, Plasma Phys. **17**, 645 (1975).

<sup>11</sup>M. Chance, S. Jardin, and T. Stix, Phys. Rev. Lett. **51**, 1963 (1983).

<sup>12</sup>J. Manickam, R. Grimm, and M. Okabayashi, Phys. Rev. Lett. **51**, 1959 (1983).

<sup>13</sup>D. Johnson *et al.*, in *Plasma Physics and Controlled Nuclear Fusion Research, 1982* (IAEA, Vienna, 1983), Vol. 1, p. 9.

<sup>14</sup>M. Okabayashi *et al.*, in *Plasma Physics and Controlled Nuclear Fusion Research, 1984* (IAEA, Vienna, 1985), Vol. 1, p. 229.

<sup>15</sup>V. D. Shafranov, Plasma Phys. **13**, 757 (1971).

<sup>16</sup>R. C. Grimm, J. M. Greene, and J. L. Johnson, Meth. Comput. Phys. **16**, 253 (1976).

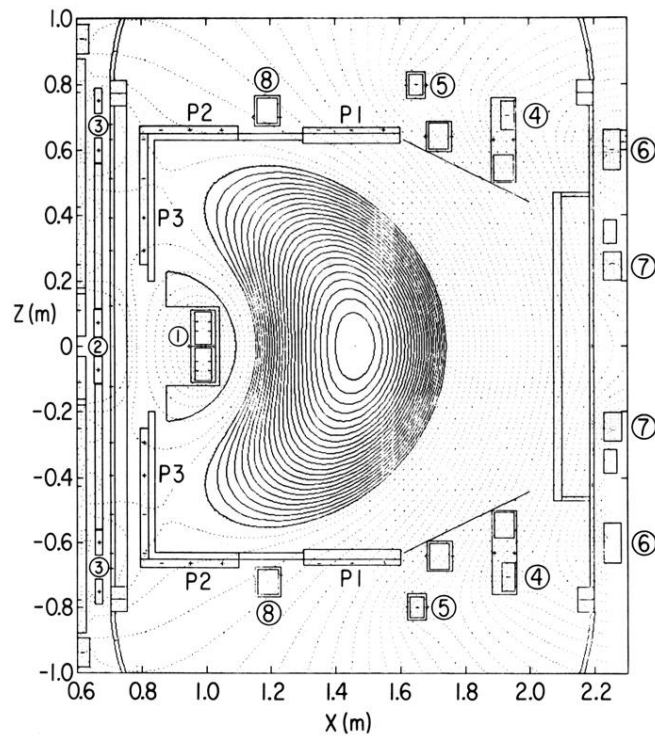


FIG. 1. Layout of PBX with magnetic field configuration for  $\beta = 5\%$ . P1-P3 are the aluminum passive stabilizers; coils 1-4 do the shaping; coils 5-7 provide radial equilibrium. Graphite armor is shown on coil 1 and the thickness of the graphite bars on P1-P3.